Study of the Si IV emission lines in the UV spectra of 21 HiBALQSOs

E. Lyratzi*, E. Danezis*, L. Č. Popović**,
A. Antoniou*,D.Stathopoulos*, M. S. Dimitrijević**
** University of Athens, ** Astronomical Observatory of Belgrade*

Active Galactic Nuclei - AGN

An Active Galactic Nucleus is defined as a compact region in the center of a galaxy, characterized by particularly high brightness in all the regions of the electromagnetic spectrum, from radio waves up to gamma rays. The galaxies hosting active galactic nuclei are called active galaxies.

It is considered that an AGN is the product of mass accumulation around a super massive black hole.

The general "group" of Active Galactic Nuclei (AGNs) includes different types of galaxies, such as Seyfert, Radiogalaxies, Quasars, Blazars etc.

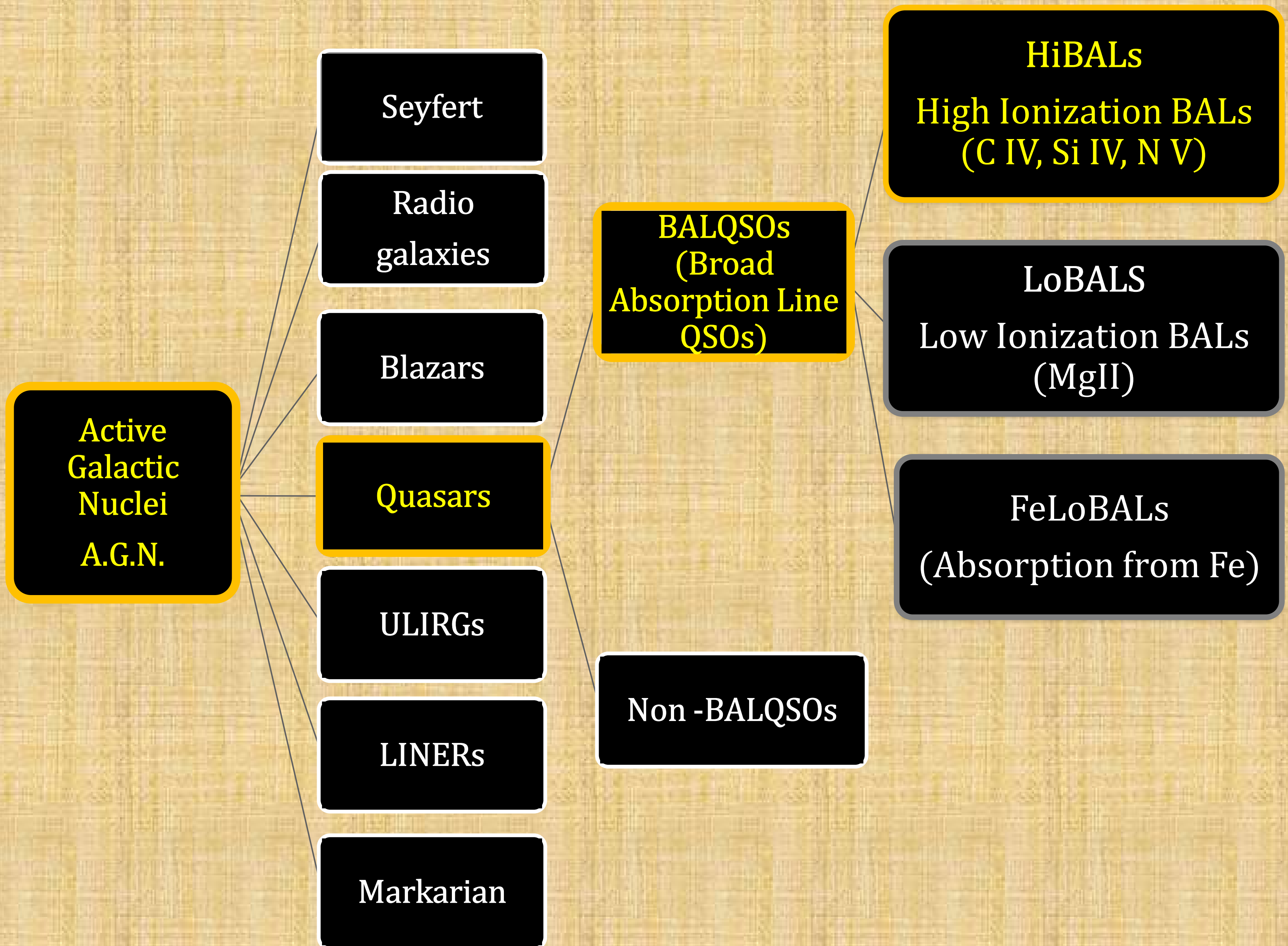
Active Galactic Nuclei
A.G.N.
Seyfert
Radio galaxies
Blazars
Quasars
ULIRGs
LINERs
Markarian
BALQSOs (Broad Absorption Line QSOs)
Non -BALQSOs
HiBALs
High Ionization BALs (C IV, Si IV, N V)
LoBALS
Low Ionization BALs (MgII)
FeLoBALs
(Absorption from Fe)

Spectral classification of BALQSOs

- *HiBALs (High Ionization BALs): BALQSOs that contain strong, broad absorption troughs short-ward of high-ionization emission lines (such as C IV, Si IV, N V) and are typically identified through the presence of C IV absorption troughs.*

- *LoBALs (Low Ionization BALs): BALQSOs that contain HiBAL features but also have absorption from low-ionization lines such as Mg II.*

- *FeLoBALs: BALQSOs with excited iron absorption features (Fe II).*

- *Non – BALs: BALQSOs with no broad absorption troughs just blueward of the C IV and Mg II emission lines.*

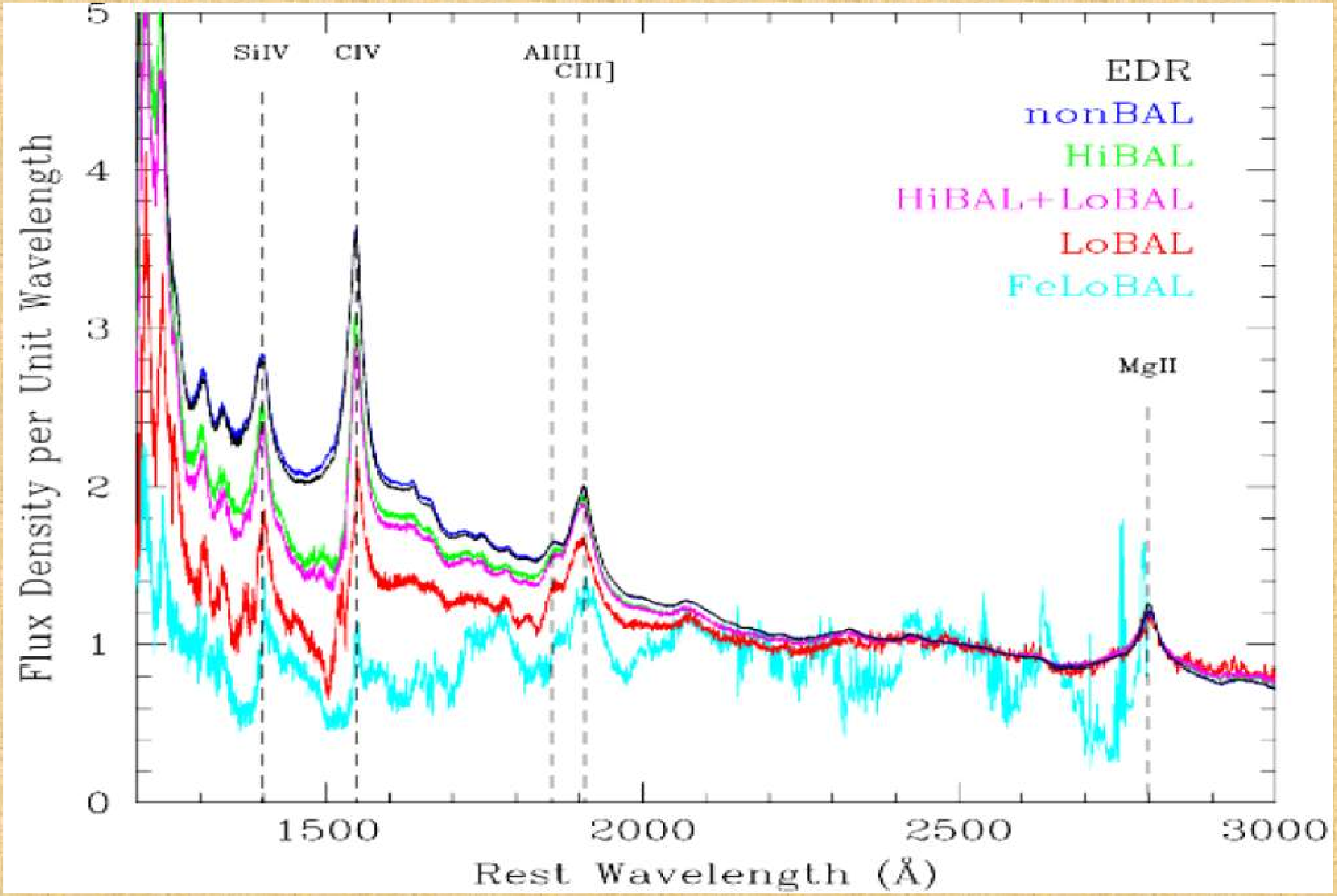

Spectral classification of QSOs (Reichard et al. 2003)

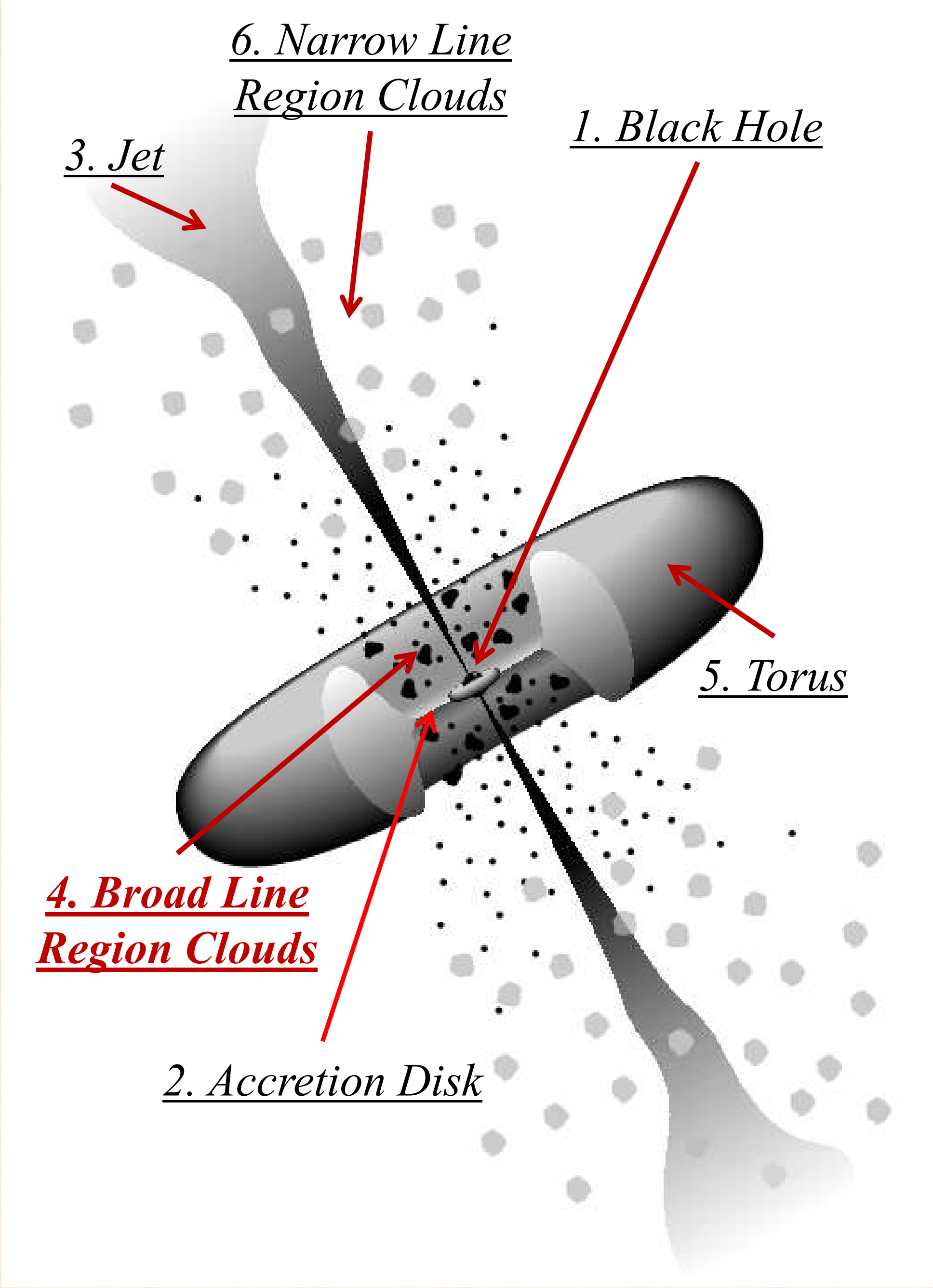

Structure

1. Black Hole
2. Accretion Disk
3. Jet
4. Broad Line Region Clouds
5. Torus
6. Narrow Line Region Clouds

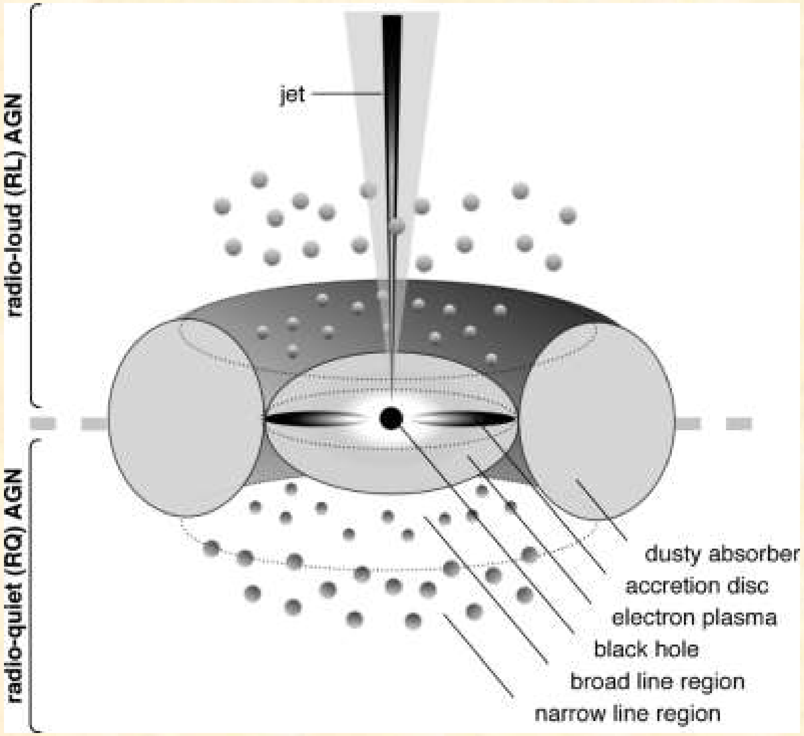

The emission lines

The broad emission lines that we observe in the optical and UV spectra of AGNs are produced in partially ionized gaseous clouds (Broad Line Clouds), which move rapidly (v>10.000 Km/sec) in the gravitation field of the black hole. This means that the broad emission lines are created in a region which is not homogeneous. *[Caroll, B. and Ostllie, D. 2006, An Introduction to Modern Astrophysics (2nd Edition)].* ***This region, which is formed by the Broad Line Clouds is called Broad Line Region (BLR) and is relatively close to the nucleus.***

It is considered that the smoothness of the observed spectral line profiles indicates the existence of a large number of clouds. *(Arav et al. 1997; Ferland 2004; Laor 2006; Laor et al. 2006).*

The study of the Fe II emission lines indicates that the temperature of the BLR is about 10^4 K.

The study of other spectral lines indicates that the numerical density of electrons lies between 10^{13} m^{-3} and 10^{16} m^{-3}.

The number the nature and the origin of these clouds are still unknown. Their mass is considered to range between 10^{-7} and 10^{-8} $M_{\odot}$ *(Peterson, B. M. 1997).* ***This value is too small to accept that the clouds are held together due to their gravitational interaction.***

Subgroups of Emission lines

In the spectra of HiBAL QSOs we detect emission lines separated in some subgroups.

1. ***Simple Emission lines (disk model or a classical distribution, such as Gauss, Lorentz and Voigt)***

2. ***Multi-component emission lines***

Simple Emission lines

The first subgroup of emission lines includes lines with simple profiles that we can fit using the accretion disk model or, a classical distribution as Gauss, Lorentz or Voigt.

Multi-component Emission Lines

The second subgroup of emission lines includes complex lines that cannot be simulated using only the accretion disk model. This means that the line profiles are not due to the accretion disk only, but there are other regions (clouds) apart from the disk that play a significant role too.

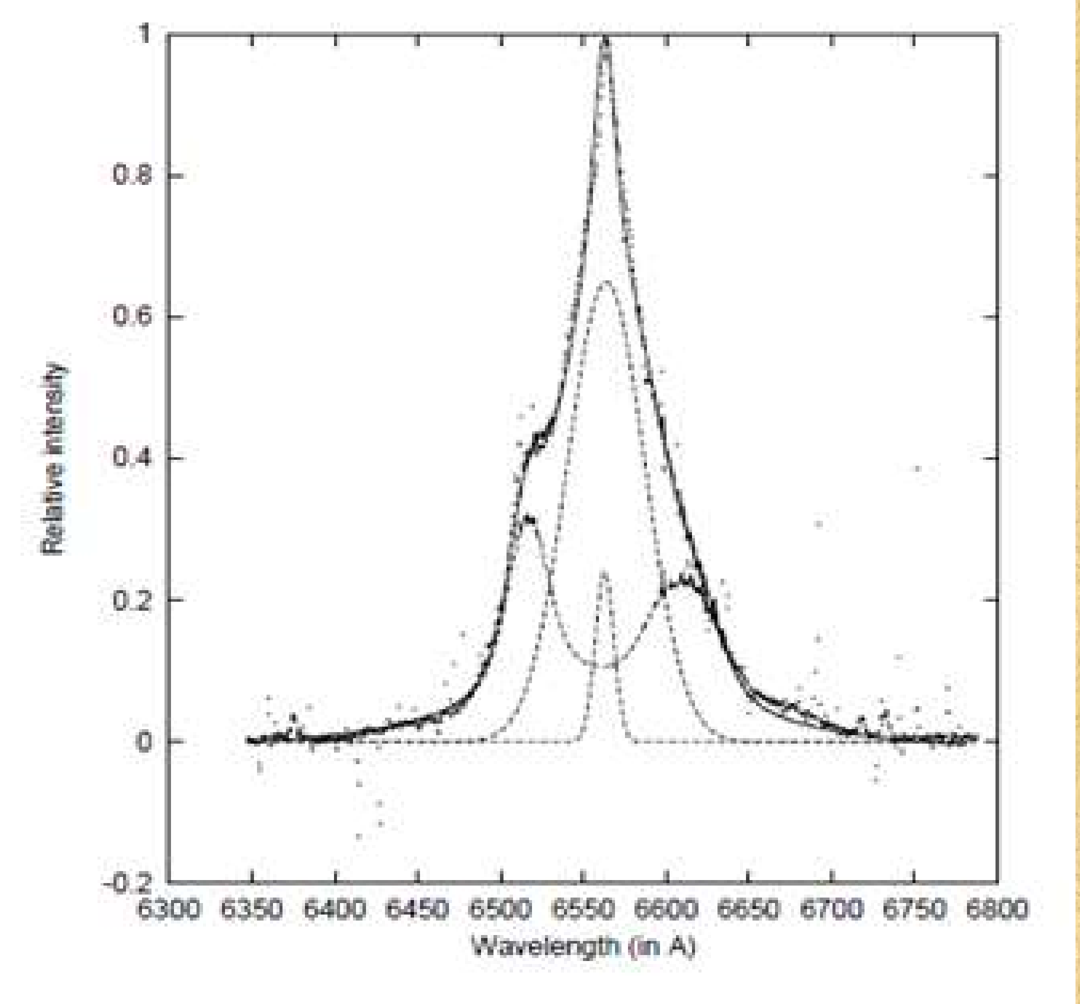

The observed Hα line (dots) fitted with multi-component model (solid line) given by Popović et al. (2002). With dashed lines the disk, broad and narrow spherical components are presented.

For the purpose of computational modeling, the BLR region is divided into two layers. These layers are the regions of HIL (High Ionization Lines) and LIL (Low Ionization Lines).

The first layer is located closer to the central source and corresponds to electron density $n_e \approx 10^{15}\ m^{-3}$.

This layer is surrounded by a second layer, which is partially ionized and has much greater electron density.

The high ionization spectral lines (Lyα, C III, C IV, Si IV, He I, He II and N V) arise from the inner layer, whereas the low ionization spectral lines, such as the lines of Balmer series and the lines of Mg II, C II and Fe II, arise from the outer layer.

Dietrich et al. (1999) studied the 3C 273 quasar and concluded that the clouds are randomly distributed in the velocity field, following a Gauss distribution.

The Gauss distribution of the velocities is characteristic for objects that are located deep in the nucleus of a giant elliptical galaxy *(Sargent et al. 1978, Harms et al. 1994).*

By applying the GR model (Gauss-Rotation model) Danezis et al. (2006, 2007, 2008) and Lyratzi et al. (2009, 2010a, 2010c) fitted the C IV resonance lines in the spectra of 30 Hi BALQSOs and showed that the BALRs and BELRs consist of a number of independent and successive density regions and that the BLRs have three apparent velocities, i.e. the velocity of outflow (radial velocity) and the rotational velocity of the density regions, as well as the random velocities of the ions, within the region.

They calculated the rotational velocities of the BLR clouds through a new distribution, the "Rotation (R) distribution". Then, they combined the two distributions (Gauss and Rotation) and they constructed a new one, the "Gauss-Rotation (GR) distribution", in order to reproduce the observed spectral line profiles of QSOs, taking into account both the random velocities (Gauss) and the rotational velocities. Through this method they were able to calculate the values of a series of physical parameters that describe the BLRs.

Using the GR model

We can calculate some important parameters of the plasma clouds that construct the components of the observed spectral feature, such as:

Direct calculations

- ***The apparent rotational velocities of absorbing or emitting density layers (V_{rot})***
- ***The apparent radial velocities of absorbing or emitting density layers (V_{rad})***
- ***The Gaussian typical deviation of the ions' random motions (σ)***
- ***The optical depth in the center of the absorption or emission components (ξ_i)***

Indirect calculations

- ***The random velocities of the ions (V_{random})***
- ***The FWHM***
- ***The absorbed or emitted energy (Ea, Ee)***
- ***The column density (CD)***

Data

In order to study the C IV resonance lines (λλ 1548.187, 1550.772 Å) we apply the GR model to the spectra of 20 broad absorption line quasars (BALQSOs) taken from the Sloan Digital Sky Survey's Data Release 7. The SDSS imaging survey uses a wide-field multi-CCD camera (Gunn et al. 1998). The spectra cover the optical range 3800–9200 Å at a resolution of 1800–2100.

In the following Table, column 1 lists the name of the QSOs, using the SDSS format of J2000.0 right ascension (hhmmss.ss) and declination (±ddmmss.s), columns 2 lists the modified Julian date-plate-fiber, column 3 lists the redshift and column 4 lists the dates of observations.

Table 1			
Object Name (SDSS)	**MJD-Plate-Fiber**	**Redshift**	**Date**
J004323.43-001552.4	51794-0393-181	2,81671	7/9/2000, 8:10
J104109.86+001051.76	51913-0274-482	2,25924	4/1/2001, 11:00
J001502.26+001212.4	51795-0389-465	2,85152	7/9/2000, 6:08
J104841.03+000042.81	51909-0276-310	2,03044	31/12/2000, 11:08
J015048.83+004126.29	51793-0402-505	3,70225	6/9/2000, 10:06
J102517.58+003422.17	51941-0272-501	1,88842	1/2/2001, 9:30
J031828.91-001523.17	51929-0413-170	1,98447	20/1/2001, 4:23
J010336.40-005508.7	51816-0396-297	2,44295	29/9/2000, 8:28
J005419.99+002727.9	51876-0394-514	2,51946	21/11/2000, 2:17
J004732.73+002111.3	51794-0393-588	2,87768	7/9/2000, 8:10
J023908.99-002121.42	51821-0408-179	3,74	4/10/2000, 9:38
J004041.39-005537.3	51794-0393-298	2,09094	7/9/2000, 8:10
J001438.28-010750.1	51795-0389-211	1,81564	7/9/2000, 6:08
J023252.80-001351.17	51820-0407-158	2,03289	3/10/2000, 9:41
J001025.90+005447.6	51795-0389-332	2,84727	7/9/2000, 6:08
J110041.20+003631.98	51908-0277-437	2,01143	30/12/2000, 11:19
J000056.89-010409.7	51791-0387-098	2,12325	4/9/2000, 7:08
J003551.98+005726.4	51793-0392-449	1,90110	6/9/2000, 8:20
J015024.44+004432.99	51793-0402-485	2,00596	6/9/2000, 10:06
J000103.85-104630.2	52143-650-133	2.081	28/2/2000 5:52
J000913.77-095754.5	52141-651-519	2.076	28/2/2000 5:52

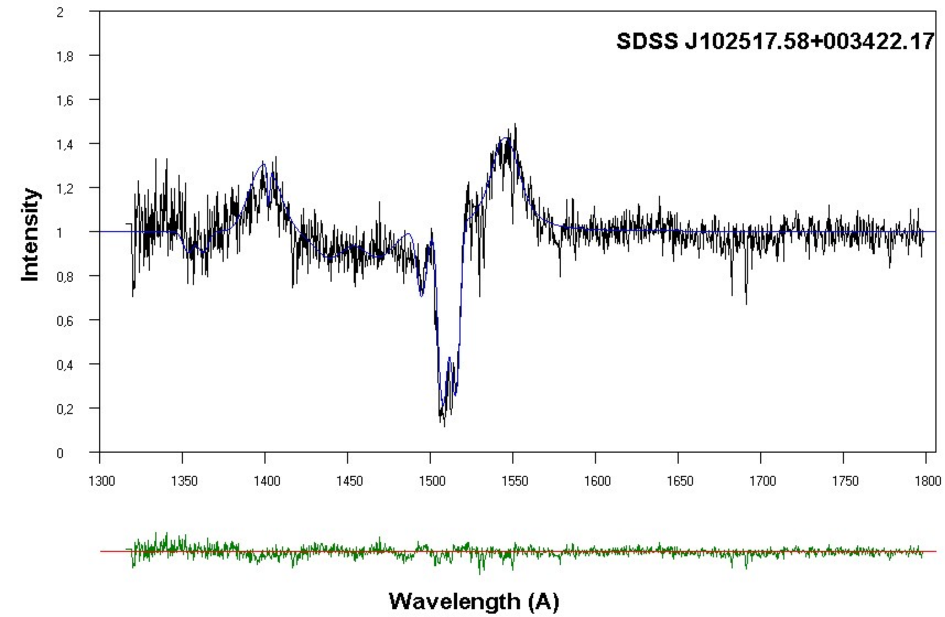
SDSS J102517.58+003422.17
Intensity
0 0,2 0,4 0,6 0,8 1 1,2 1,4 1,6 1,8 2
1300 1350 1400 1450 1500 1550 1600 1650 1700 1750 1800
Wavelength (A)

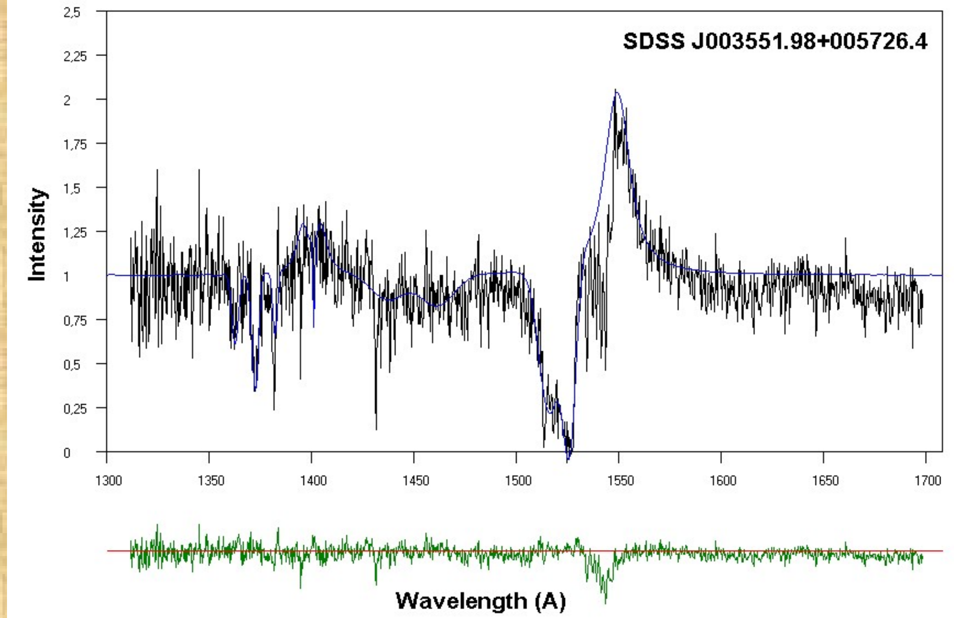
SDSS J003551.98+005726.4
Intensity
0 0,25 0,5 0,75 1 1,25 1,5 1,75 2 2,25 2,5
1300 1350 1400 1450 1500 1550 1600 1650 1700
Wavelength (A)

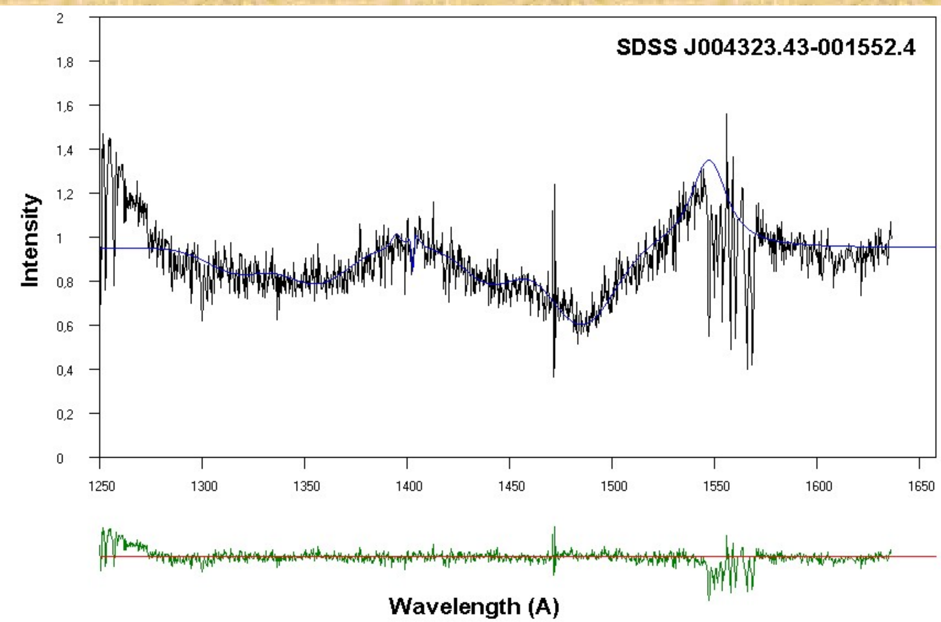
SDSS J004323.43-001552.4
Intensity
0 0,2 0,4 0,6 0,8 1 1,2 1,4 1,6 1,8 2
1250 1300 1350 1400 1450 1500 1550 1600 1650
Wavelength (A)

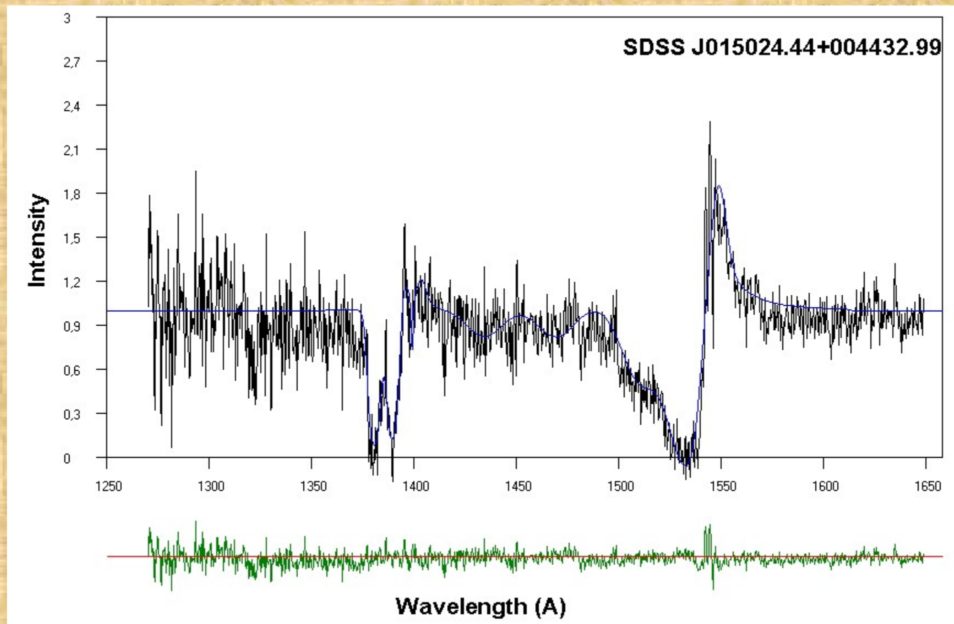
SDSS J015024.44+004432.99
Intensity
0 0,3 0,6 0,9 1,2 1,5 1,8 2,1 2,4 2,7 3
1250 1300 1350 1400 1450 1500 1550 1600 1650
Wavelength (A)

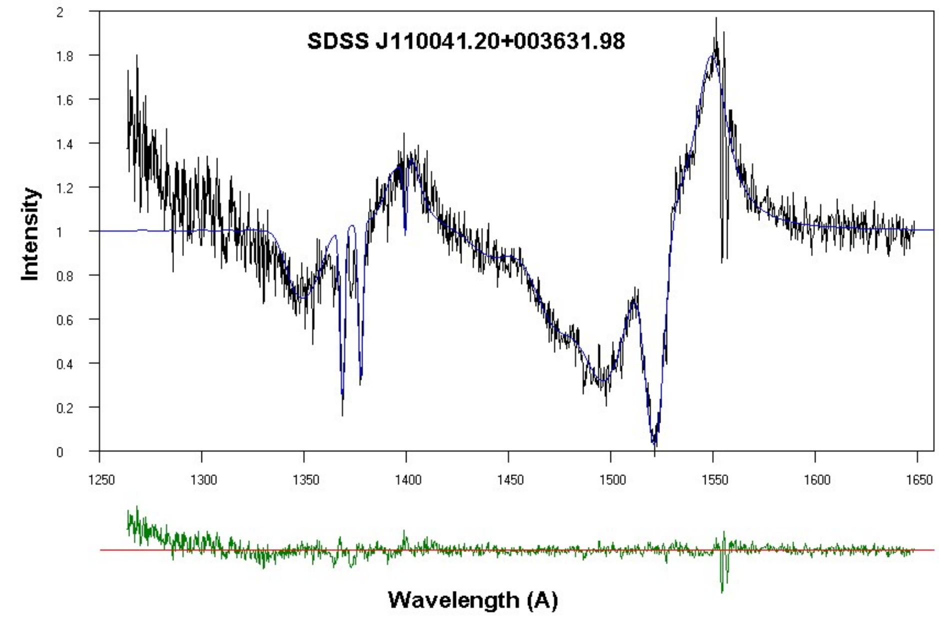
SDSS J110041.20+003631.98
Intensity
Wavelength (A)

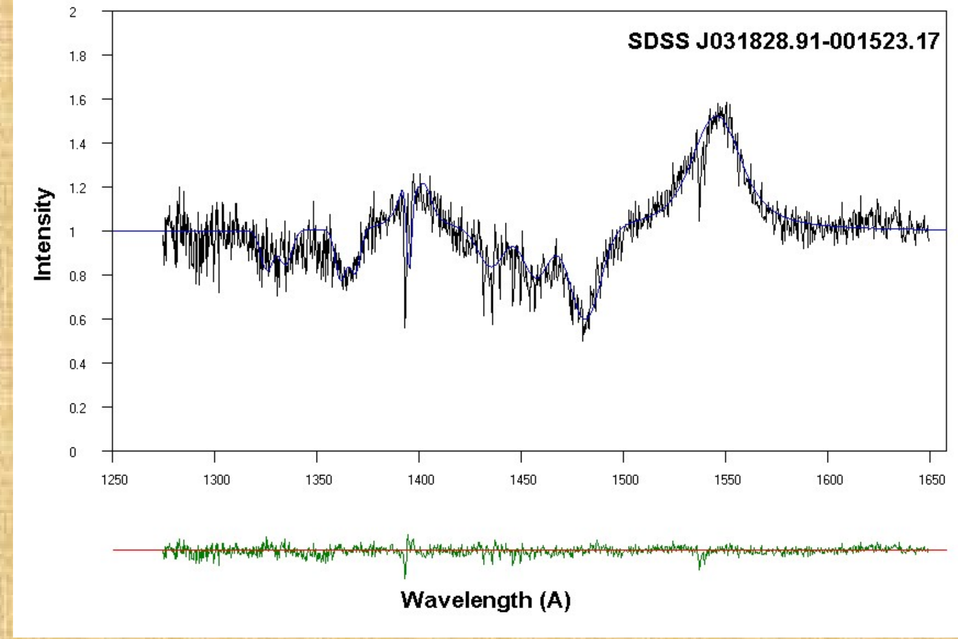
SDSS J031828.91-001523.17
Intensity
Wavelength (A)

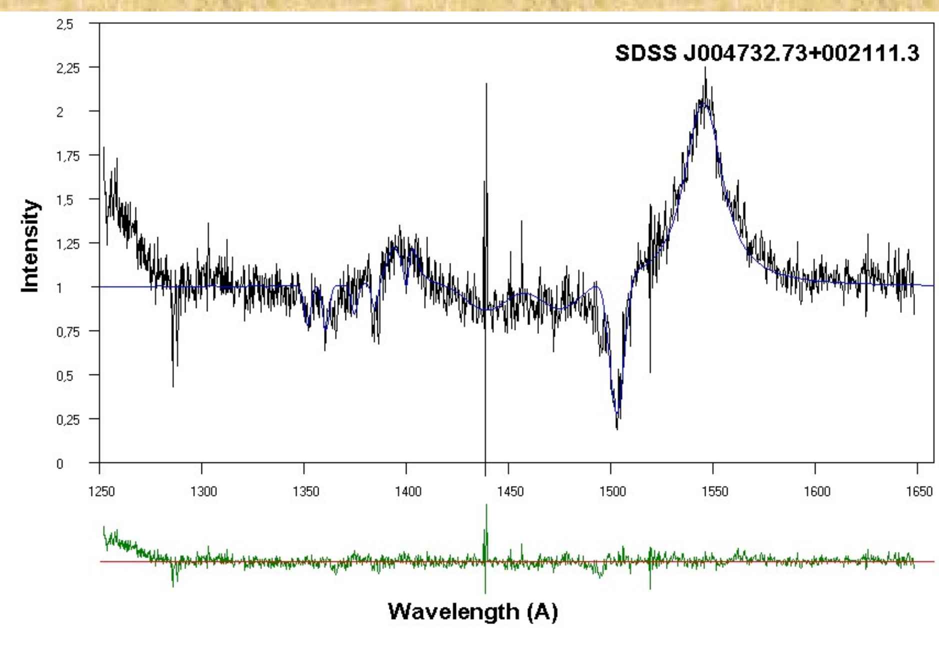
SDSS J004732.73+002111.3
Intensity
Wavelength (A)

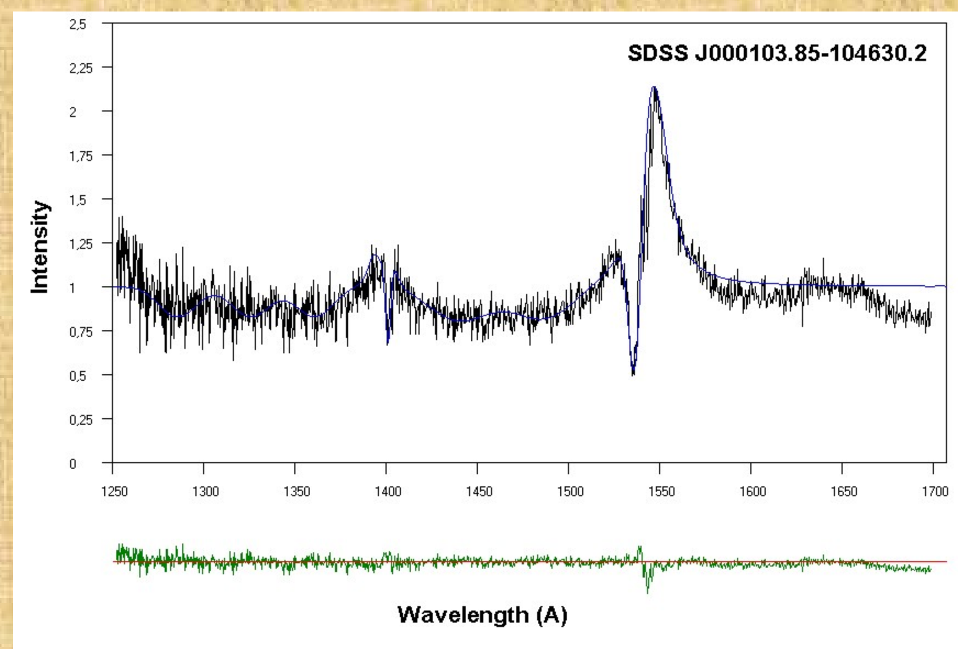
SDSS J000103.85-104630.2
Intensity
Wavelength (A)

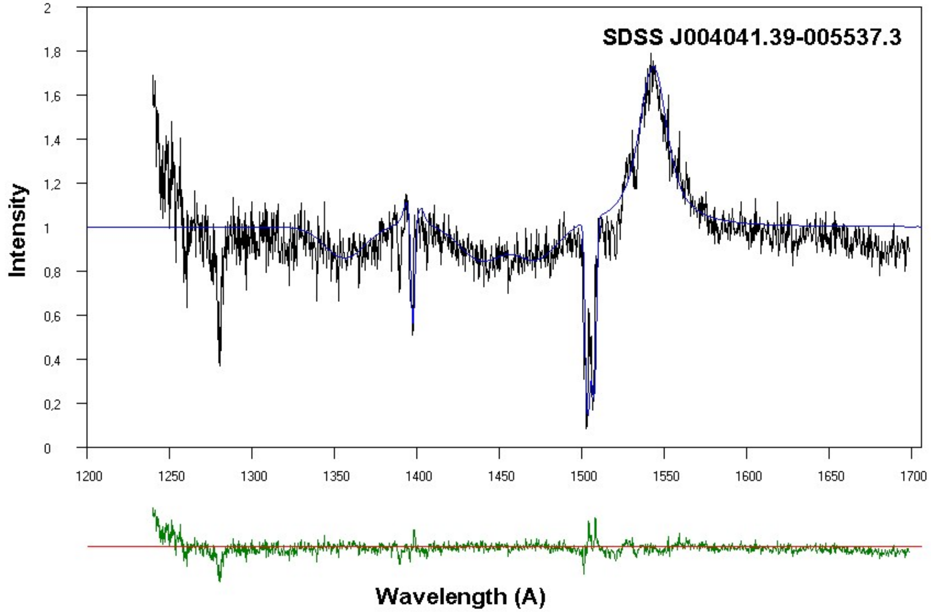
SDSS J004041.39-005537.3
Intensity
Wavelength (A)

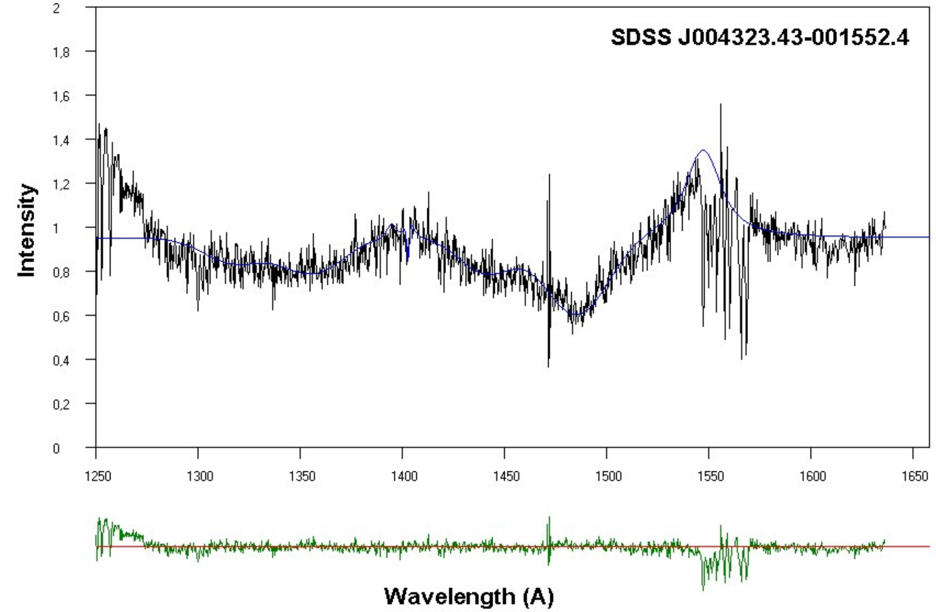
SDSS J004323.43-001552.4
Intensity
Wavelength (A)

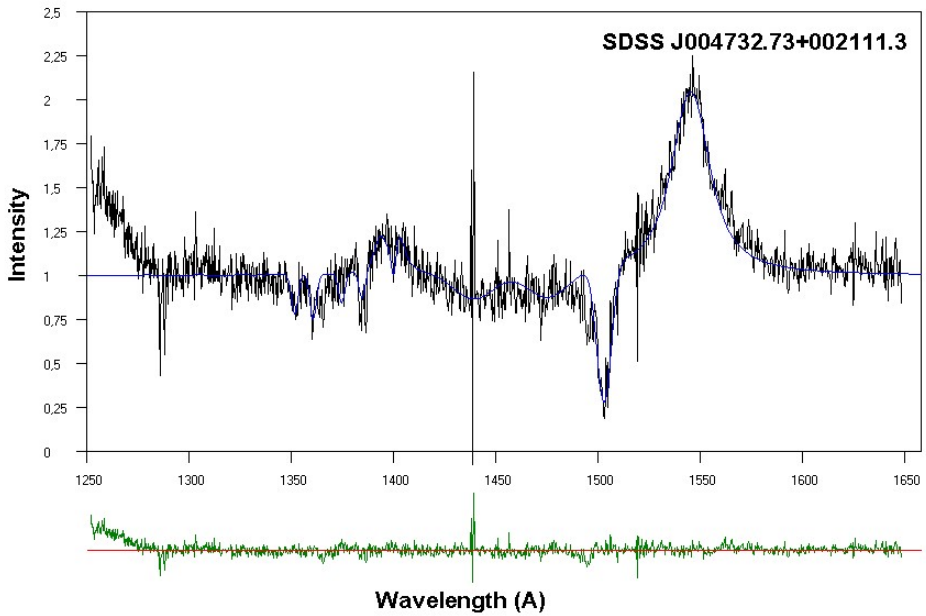
SDSS J004732.73+002111.3
Intensity
Wavelength (A)

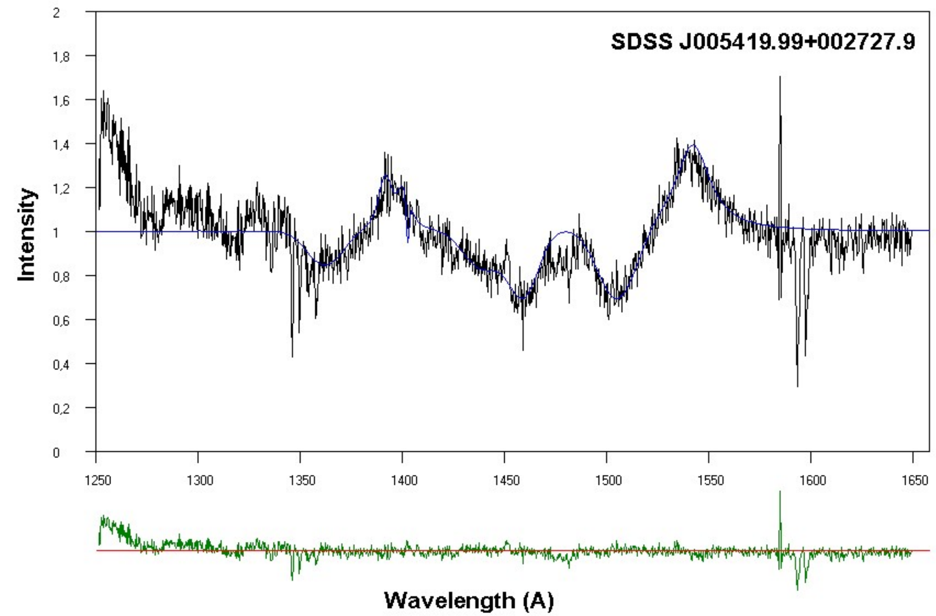
SDSS J005419.99+002727.9
Intensity
Wavelength (A)

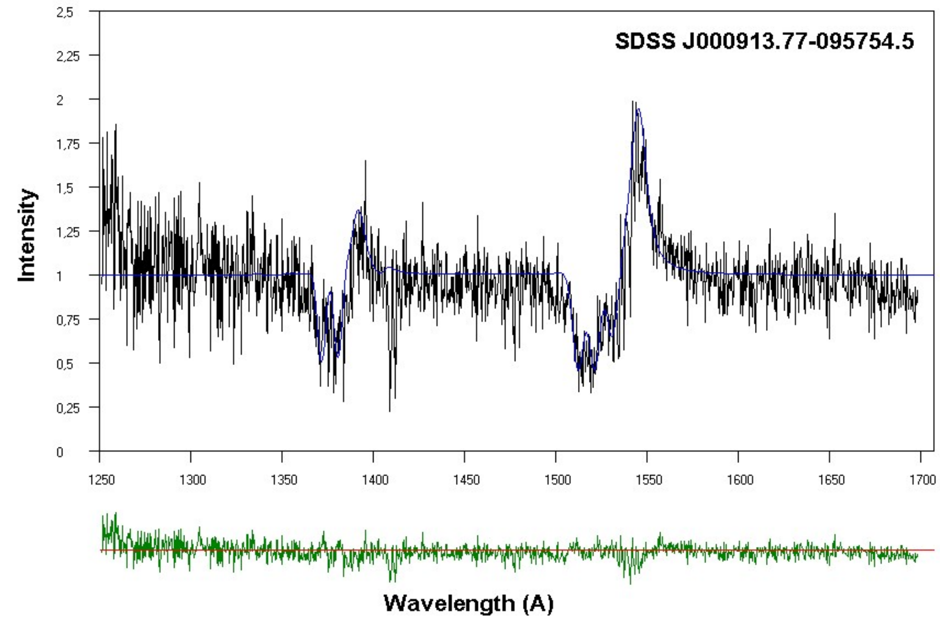
SDSS J000913.77-095754.5
Intensity
0 0,25 0,5 0,75 1 1,25 1,5 1,75 2 2,25 2,5
1250 1300 1350 1400 1450 1500 1550 1600 1650 1700
Wavelength (A)

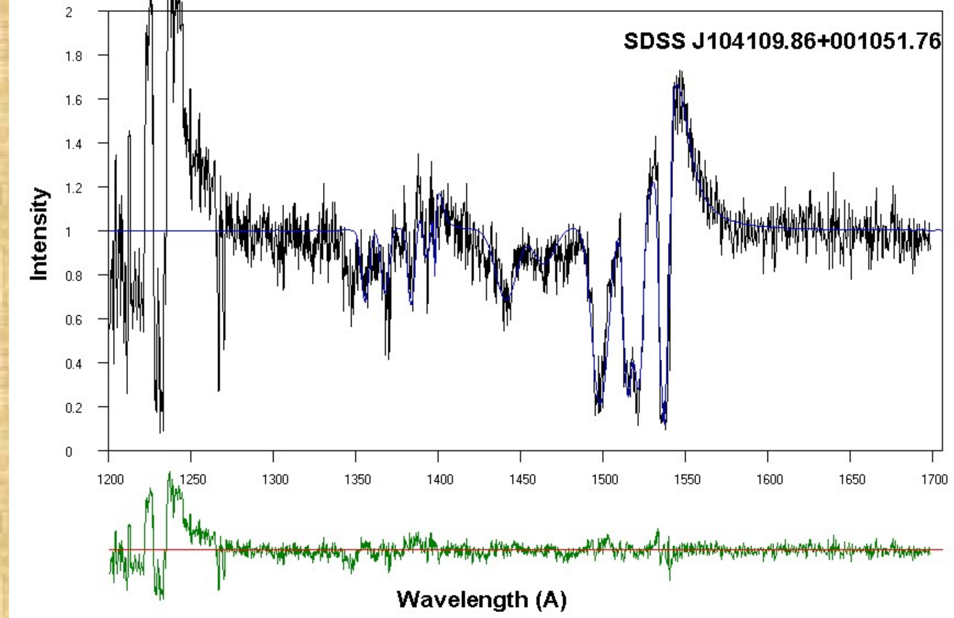
SDSS J104109.86+001051.76
Intensity
0 0.2 0.4 0.6 0.8 1 1.2 1.4 1.6 1.8 2
1200 1250 1300 1350 1400 1450 1500 1550 1600 1650 1700
Wavelength (A)

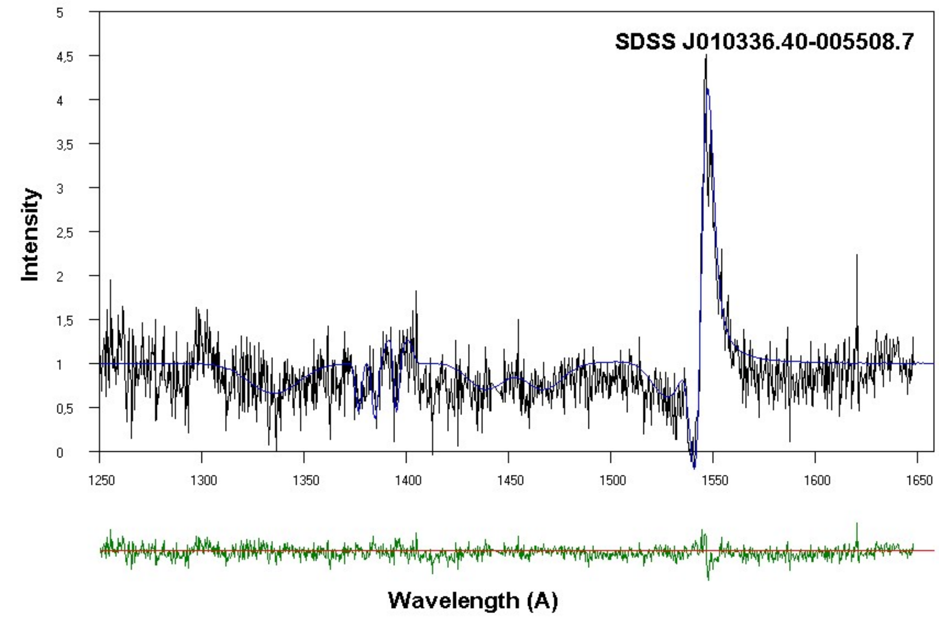
SDSS J010336.40-005508.7
Intensity
0 0,5 1 1,5 2 2,5 3 3,5 4 4,5 5
1250 1300 1350 1400 1450 1500 1550 1600 1650
Wavelength (A)

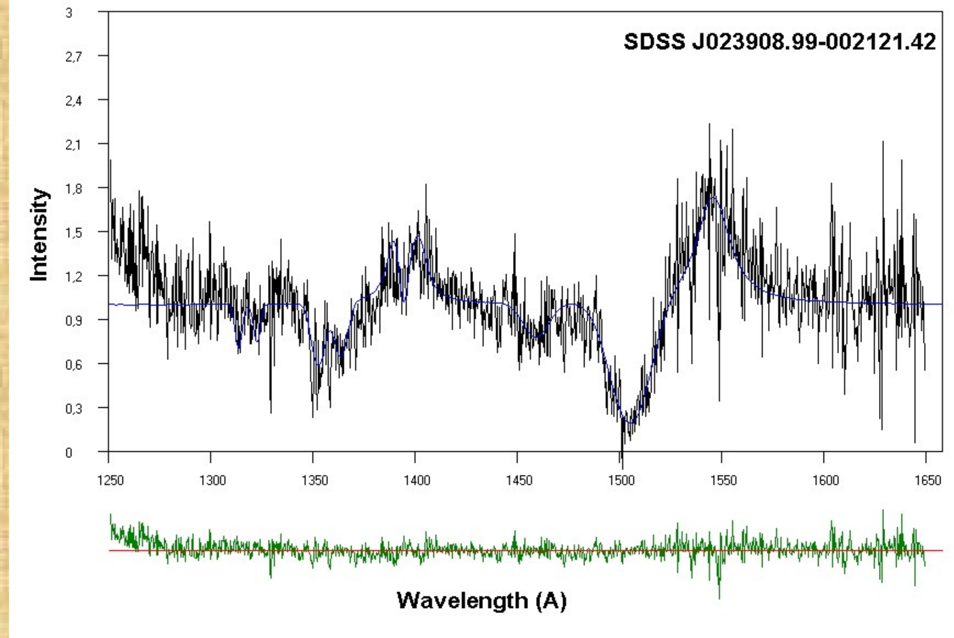
SDSS J023908.99-002121.42
Intensity
0 0,3 0,6 0,9 1,2 1,5 1,8 2,1 2,4 2,7 3
1250 1300 1350 1400 1450 1500 1550 1600 1650
Wavelength (A)

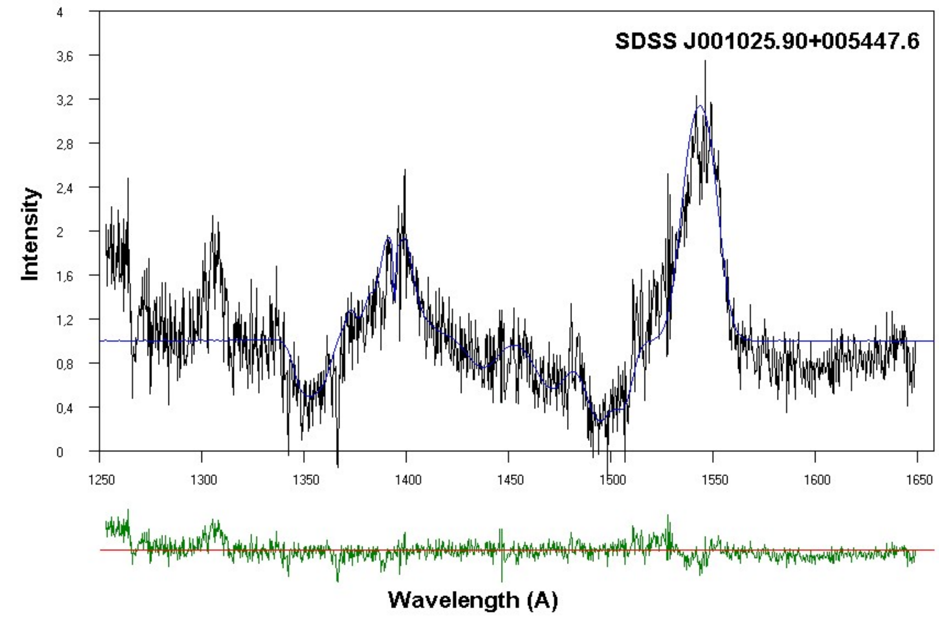
SDSS J001025.90+005447.6
Intensity
Wavelength (A)

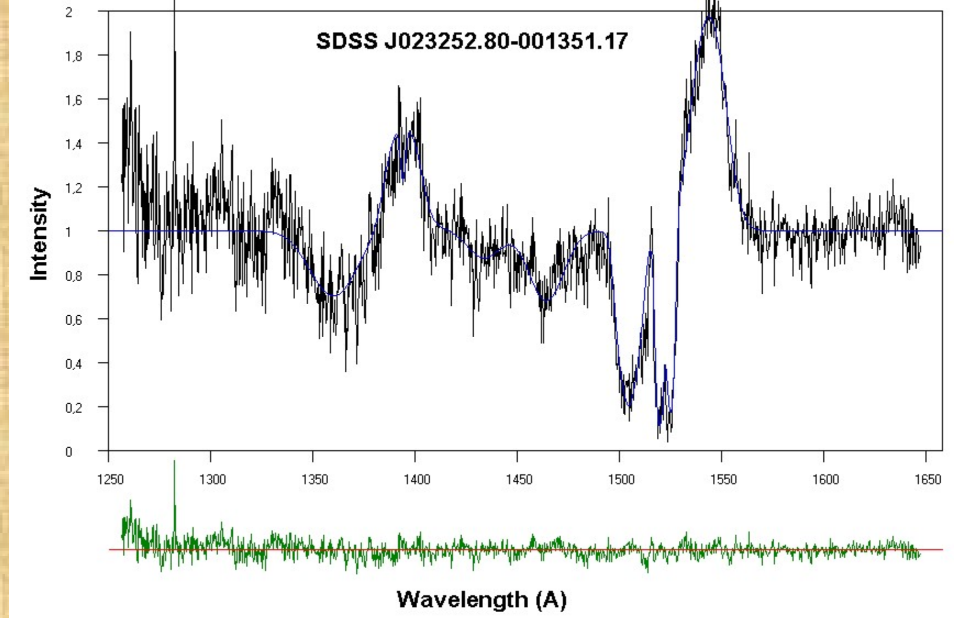
SDSS J023252.80-001351.17
Intensity
Wavelength (A)

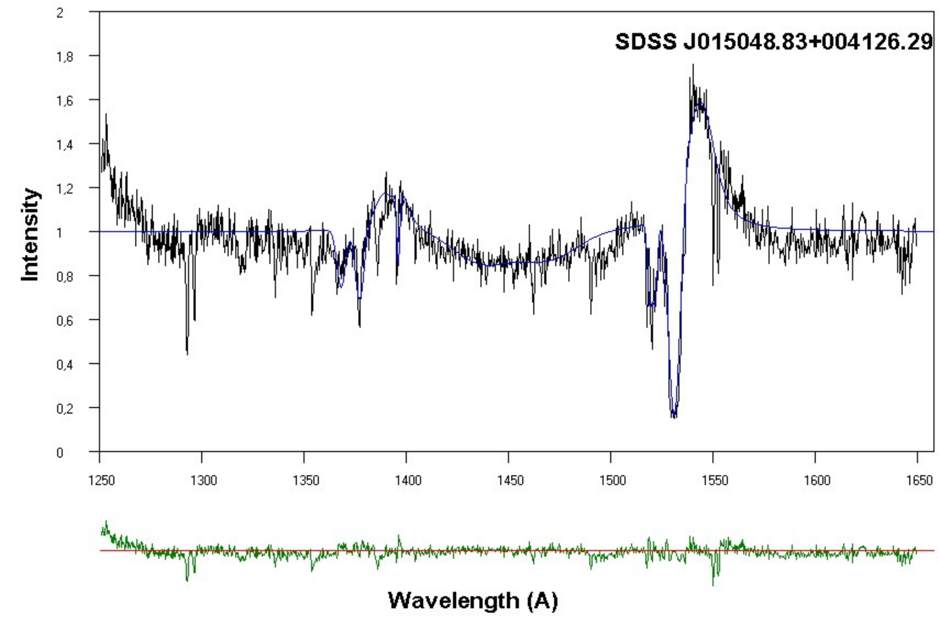
SDSS J015048.83+004126.29
Intensity
Wavelength (A)

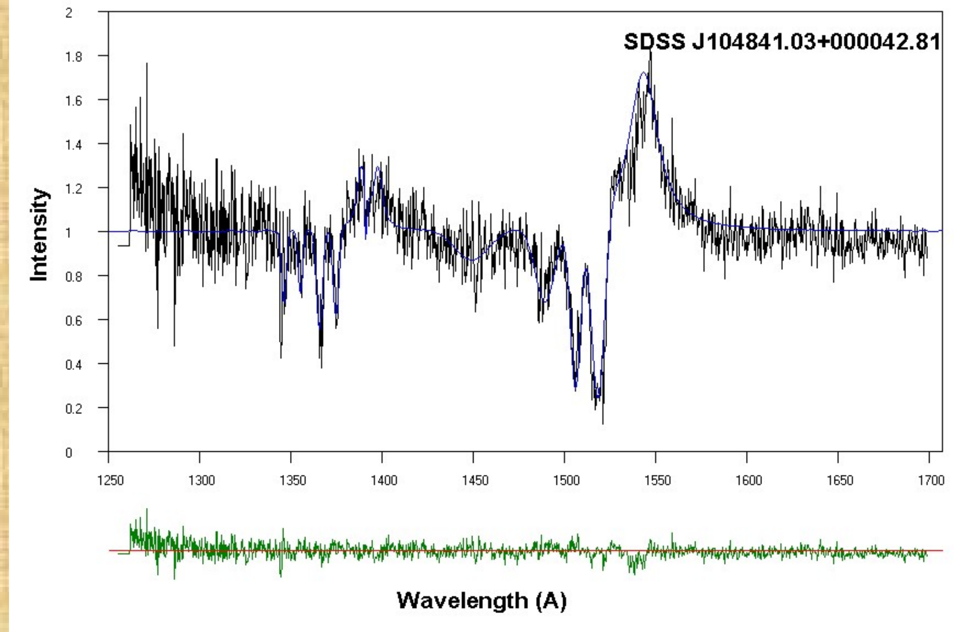
SDSS J104841.03+000042.81
Intensity
Wavelength (A)

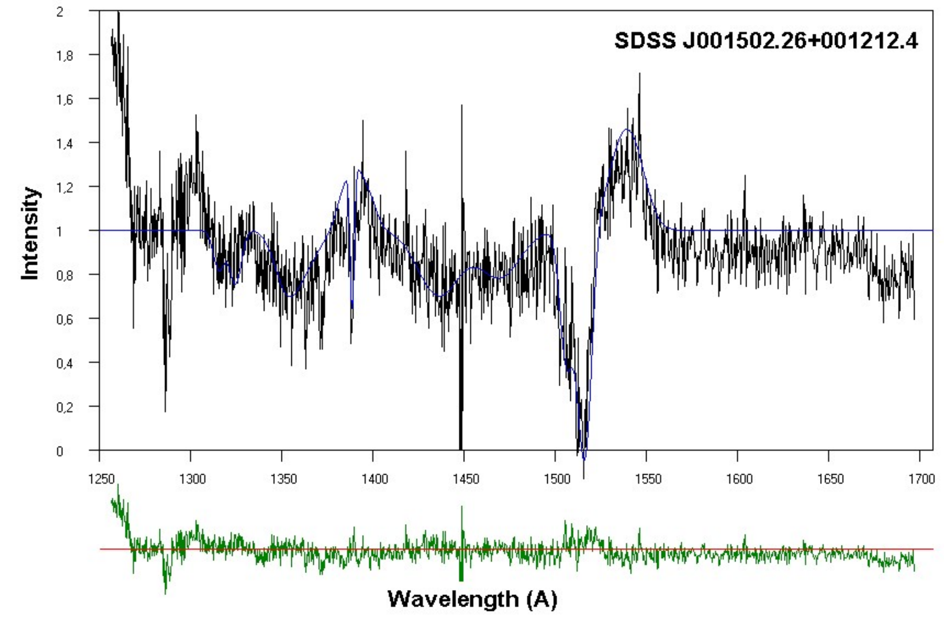
SDSS J001502.26+001212.4
Intensity
Wavelength (A)
2
1,8
1,6
1,4
1,2
1
0,8
0,6
0,4
0,2
0
1250
1300
1350
1400
1450
1500
1550
1600
1650
1700

Conclusions

Object Name (SDSS)	Red Shift	Vrad (km/s)	Vrand (km/s)	ξ	σ	γ	FWHM (Å)	CD (cm^{-2})	E (eV)
J102517.58+003422.17	1.88842	428.81	1768.33	0.450	7.0		17.835	8.42E+09	3.36
J003551.98+005726.4	1.9011	428.81	1009.03	0.300	4.0	0.6	7.026	6.93E+09	2.76
J004323.43-001552.4	2.81671	214.41	757.31	0.270	3.0	0.7	5.345	1.27E+09	0.51
J015024.44+004432.99	2.00596	214.41	757.31	0.500	3.0	1.0	5.992	4.06E+09	1.62
J110041.20+003631.98	2.01143	0.00	1515.71	0.550	6.0	0.7	11.392	9.89E+09	3.94
J031828.91-001523.17	1.98447	0.00	1263.09	0.463	5.0	0.6	9.128	6.42E+09	2.56
J004732.73+002111.3	2.87768	0.00	1010.47	0.500	4.0	0.7	7.509	5.50E+09	2.19
J000103.85-104630.2	2.081	0.00	1010.47	0.426	4.0	1.4	8.558	3.96E+09	1.58
J004041.39-005537.3	2.09094	0.00	757.85	0.325	3.0	0.6	5.343	1.83E+09	0.73
J000056.89-010409.7	2.12325	0.00	593.94	0.800	2.4	1.0	4.985	9.47E+09	3.78
J001438.28-010750.1	1.81564	0.00	227.36	0.925	0.9	1.6	2.158	1.97E+09	0.79
J005419.99+002727.9	2.51946	-428.81	1011.92	0.509	4.0	1.0	8.004	5.62E+09	2.24
J000913.77-095754.5	2.076	-428.81	1011.92	0.629	4.0	1.0	8.201	8.34E+09	3.32
J104109.86+001051.76	2.25924	-428.81	885.43	0.463	3.5	0.8	6.658	4.15E+09	1.66
J010336.40-005508.7	2.44295	-428.81	505.24	0.600	2.0		5.225	3.71E+09	1.48
J023908.99-002121.42	3.74	-429.50	1264.91	0.740	5.0	0.7	9.905	1.54E+10	6.12
J001025.90+005447.6	2.84727	-643.22	1265.81	1.100	5.0	0.4	10.484	2.94E+10	11.73
J023252.80-001351.17	2.03289	-857.63	1266.72	0.700	5.0	2.2	12.246	1.22E+10	4.86
J015048.83+004126.29	3.70225	-1072.03	1267.62	0.450	5.0	1.0	9.885	4.93E+09	1.96
J104841.03+000042.81	2.03044	-1072.03	760.57	0.600	3.0	0.6	5.656	5.84E+09	2.33
J001502.26+001212.4	2.85152	-1500.84	1263.09	0.463	5.0		12.766	6.60E+09	2.63

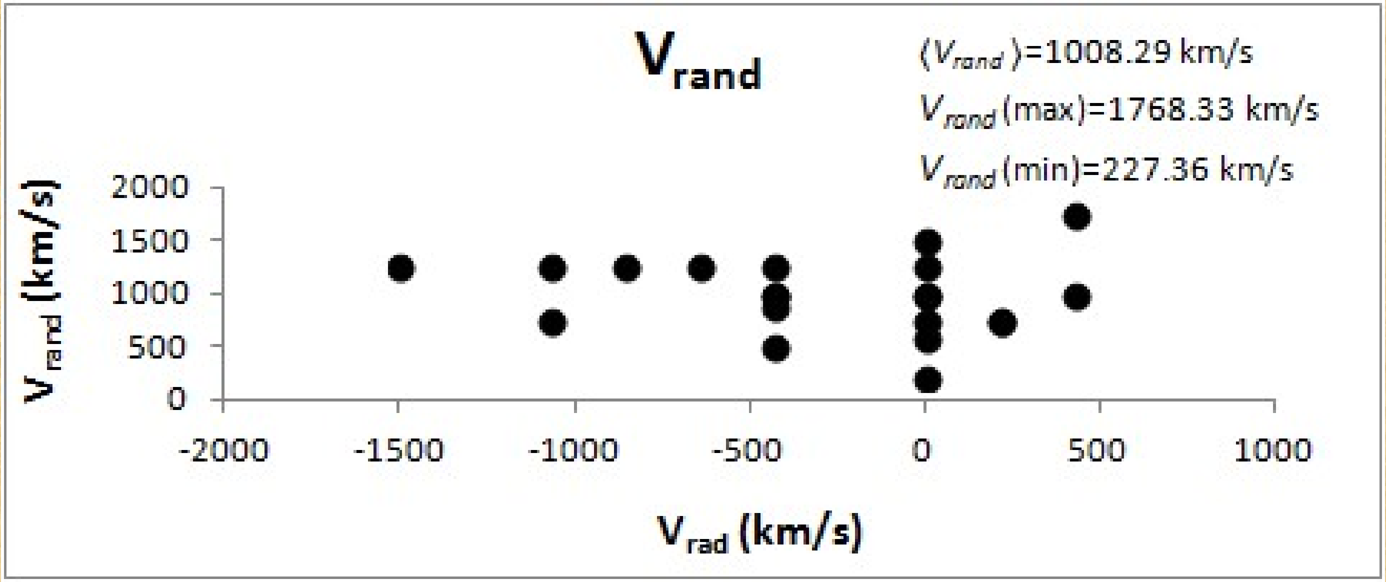

V_{rand}
$\langle V_{rand} \rangle$=1008.29 km/s
V_{rand}(max)=1768.33 km/s
V_{rand}(min)=227.36 km/s
V_{rand} (km/s)
2000
1500
1000
500
0
-2000
-1500
-1000
-500
0
500
1000
V_{rad} (km/s)

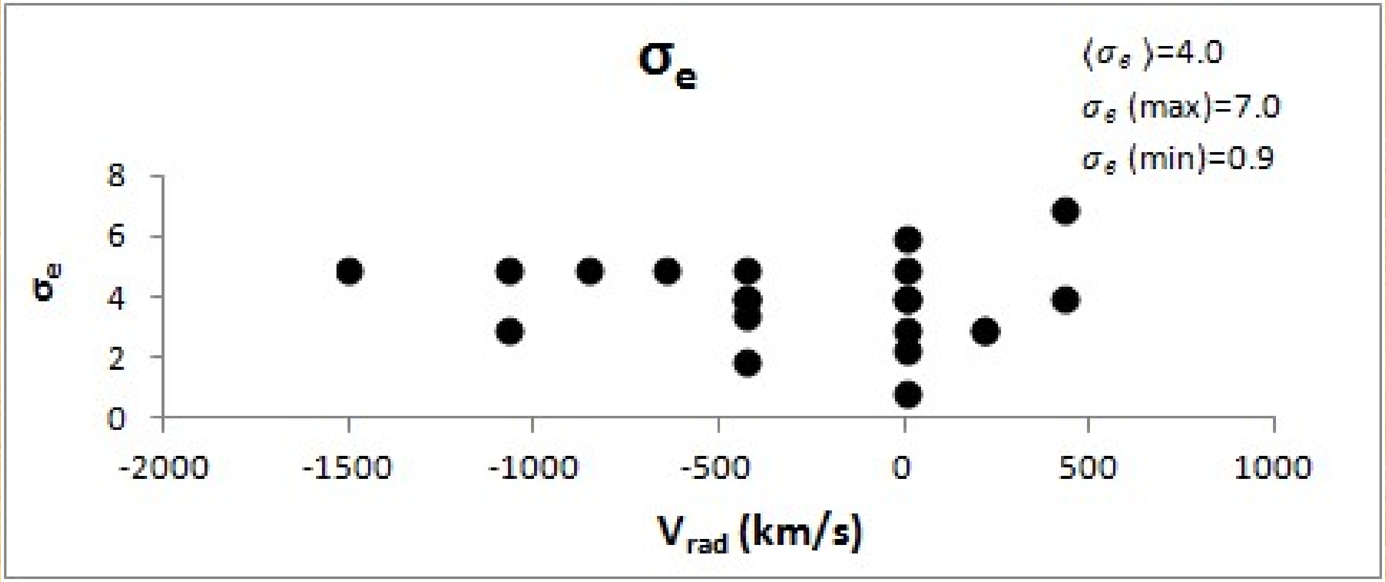

σ_e
$\langle \sigma_e \rangle$=4.0
σ_e (max)=7.0
σ_e (min)=0.9
σ_e
8
6
4
2
0
-2000
-1500
-1000
-500
0
500
1000
V_{rad} (km/s)

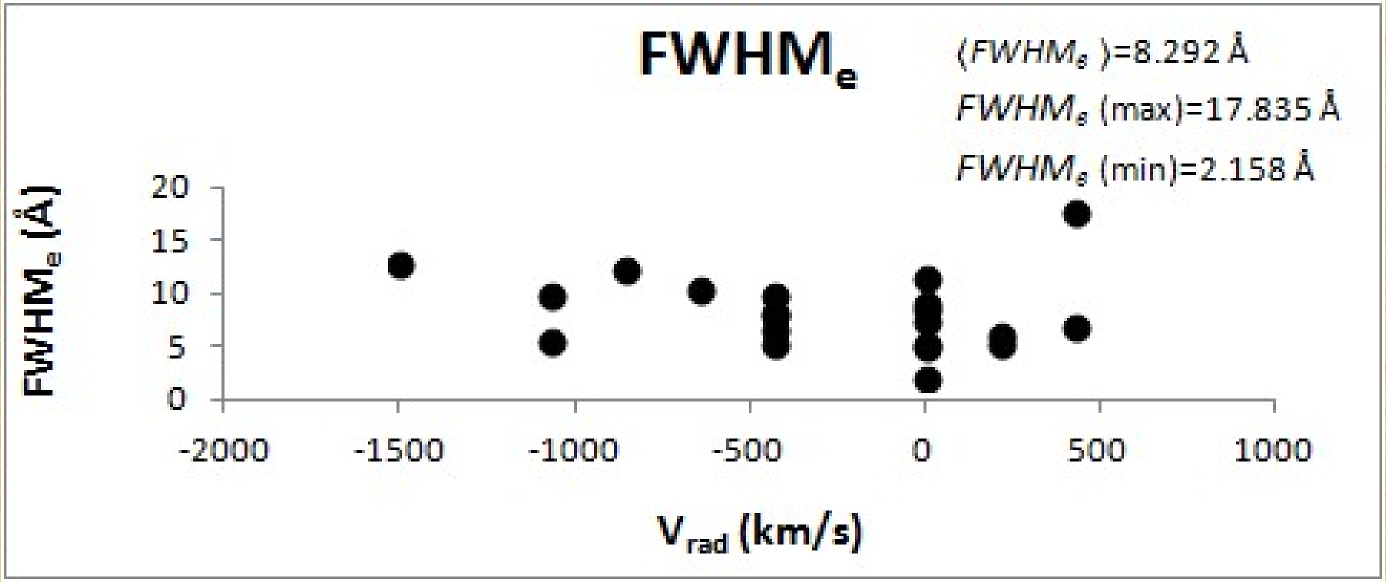
FWHMe
⟨FWHMe⟩=8.292 Å
FWHMe (max)=17.835 Å
FWHMe (min)=2.158 Å
FWHMe (Å)
20
15
10
5
0
-2000
-1500
-1000
-500
0
500
1000
Vrad (km/s)

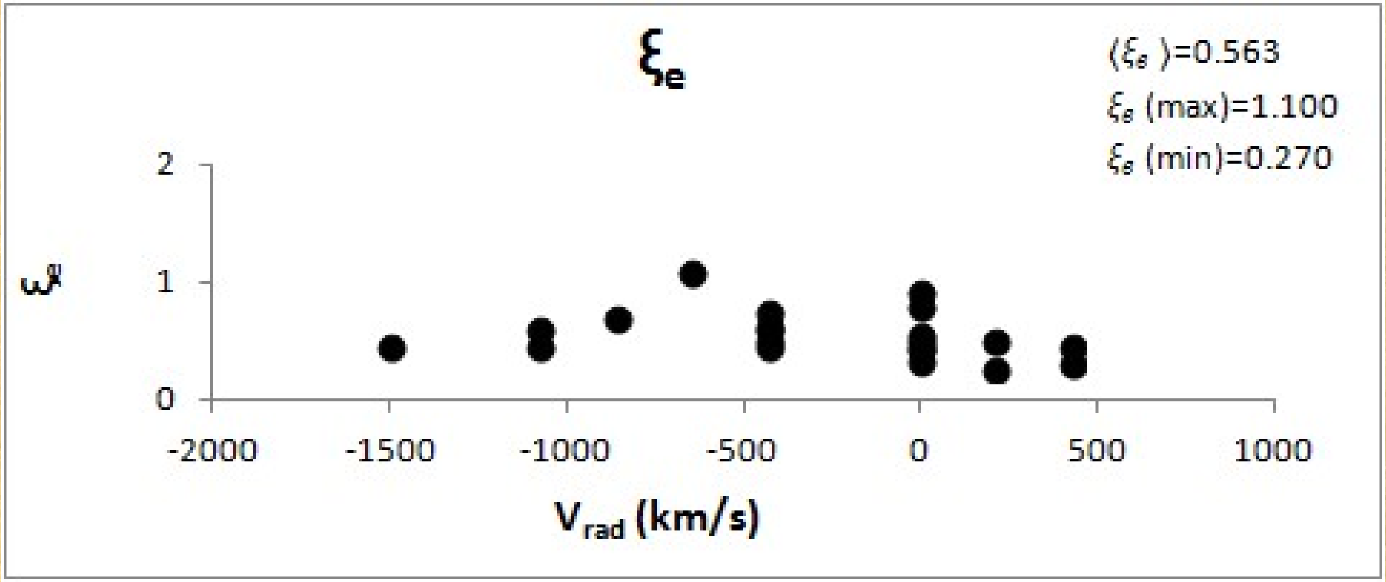
ξe
⟨ξe⟩=0.563
ξe (max)=1.100
ξe (min)=0.270
ξe
2
1
0
-2000
-1500
-1000
-500
0
500
1000
Vrad (km/s)

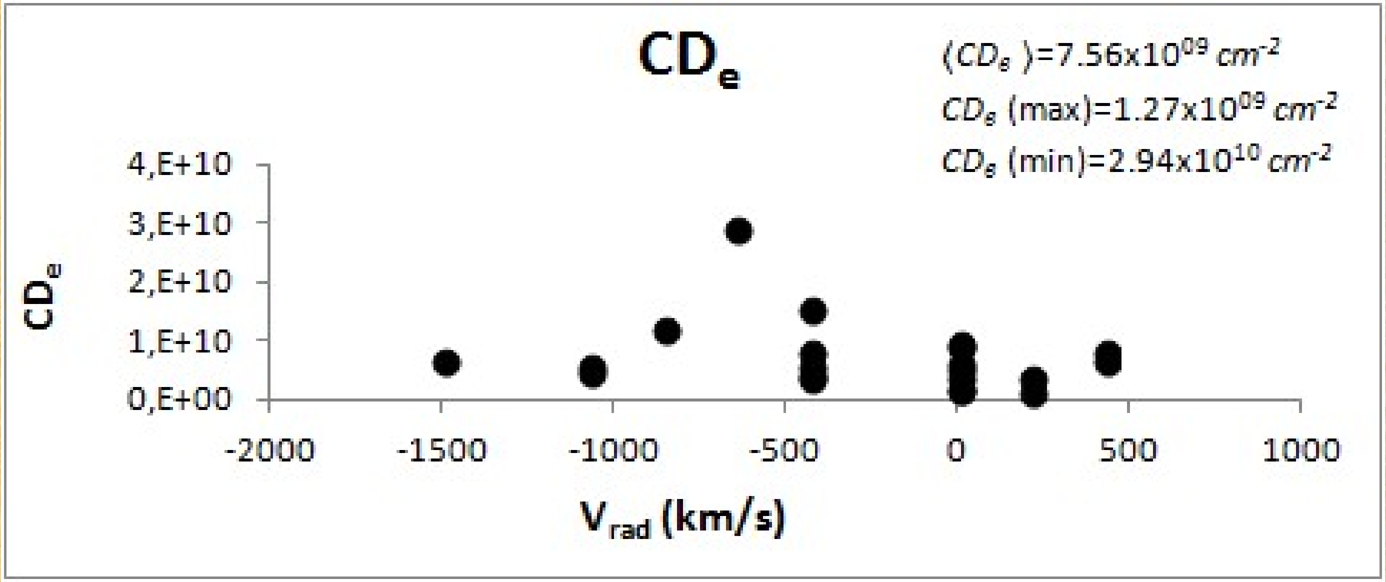
CDe
⟨CDe⟩=7.56x10^09 cm^-2
CDe (max)=1.27x10^09 cm^-2
CDe (min)=2.94x10^10 cm^-2
4,E+10
3,E+10
2,E+10
1,E+10
0,E+00
CDe
-2000
-1500
-1000
-500
0
500
1000
Vrad (km/s)

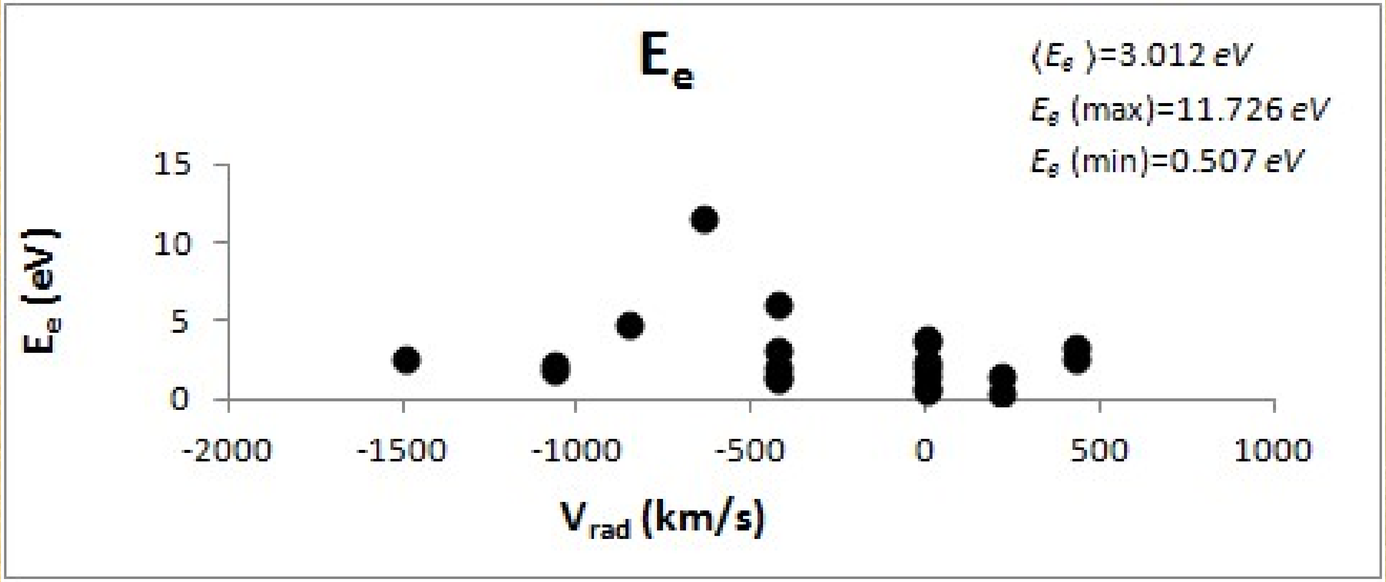
Ee
⟨Ee⟩=3.012 eV
Ee (max)=11.726 eV
Ee (min)=0.507 eV
15
10
5
0
Ee (eV)
-2000
-1500
-1000
-500
0
500
1000
Vrad (km/s)

2. After a detailed analysis of the absorption spectra lines of the same sum of 21 HiBALQSOs (see the presentation of Mr Stathopoylos pote egine…) we conclude that all resonance CIV emission spectral lines, present p Cyg profiles. This means that in a future work we should try to calculate the mass loss from the regions that create these emission lines.

3. We fitted (simulated) all the resonance C IV emission lines with a Voigt distribution. This means that in the disc (or cloud) region that produces the C IV resonance lines, pressure exists, perhaps able to create a sock (Fromerth & Melia 2001) due to great decrease of the kinematic energy and that is the reason of the radiant energy.

4. As we can see we simulated the CIV emission lines with a Voigt distribution, i.e. with a distribution with one pick.
   In the case that the emission lines arise prom an emission disc (Holt et al. 1992 (Collin-Souffrin 1987, Collin & Hure 2001) , we know that the disc model indicates such a shape only when the observation line and the rotational axis of the disc form a small angle (between 0-5 degrees).**(see Antonucci, R. 1993).**